Atomic force microscopic imaging of seeded fibril formation and fibril branching by the Alzheimer's disease amyloid-β protein

James D Harper[1,2], Charles M Lieber[3] and Peter T Lansbury, Jr[2]

Background: Amyloid plaques composed of the fibrillar form of the amyloid-β protein (Aβ) are the defining neuropathological feature of Alzheimer's disease (AD). A detailed understanding of the time course of amyloid formation could define steps in disease progression and provide targets for therapeutic intervention. Amyloid fibrils, indistinguishable from those derived from an AD brain, can be produced *in vitro* using a seeded polymerization mechanism. In its simplest form, this mechanism involves a cooperative transition from monomeric Aβ to the amyloid fibril without the buildup of intermediates. Recently, however, a transient species, the Aβ amyloid protofibril, has been identified. Here, we report studies of Aβ amyloid protofibril and its seeded transition into amyloid fibrils using atomic force microscopy.

Results: Seeding of the protofibril-to-fibril transition was observed. Preformed fibrils, but not protofibrils, effectively seeded this transition. The assembly state of Aβ influenced the rate of seeded growth, indicating that protofibrils are fibril assembly precursors. The handedness of the helical surface morphology of fibrils depended on the chirality of Aβ. Finally, branched and partially wound fibrils were observed.

Conclusions: The temporal evolution of morphologies suggests that the protofibril-to-fibril transition is nucleation-dependent and that protofibril winding is involved in that transition. Fibril unwinding and branching may be essential for the post-nucleation growth process. The protofibrillar assembly intermediate is a potential target for AD therapeutics aimed at inhibiting amyloid formation and AD diagnostics aimed at detecting presymptomatic disease.

Addresses: [1]Department of Chemistry, Massachusetts Institute of Technology, Cambridge, MA 02139, USA. [2]Center for Neurologic Diseases, Brigham and Women's Hospital and Harvard Medical School, 77 Ave Louis Pasteur, Boston, MA 02115, USA. [3]Department of Chemistry and Chemical Biology, Harvard University, 12 Oxford St. Cambridge, MA 02138, USA.

Correspondence: CM Lieber or PT Lansbury
E-mail: cml@cmliris.harvard.edu
lansbury@cnd.bwh.harvard.edu

Key words: Alzheimer's disease, amyloid, atomic force microscopy, nucleation, protofibril seeding

Received: **17 October 1997**
Accepted: **4 November 1997**

Chemistry & Biology December 1997, 4:951–959
http://biomednet.com/elecref/1074552100400951

Introduction

Amyloid plaque in the brain is the unique and defining feature of Alzheimer's disease (AD) and convergent evidence strongly suggests that it plays a central role in the pathogenesis of AD [1–3]. Thus, endogenous factors that increase the rate of amyloid formation could accelerate the onset of AD, whereas those that inhibit amyloid formation may delay its onset and slow its progression. Elucidation of the mechanism of amyloid fibril formation would facilitate the design of compounds that inhibit amyloid formation (potential therapeutic agents) [4] or detect and report its early stages (potential diagnostic agents) [2].

The insoluble fibrillar core of the AD amyloid plaque comprises variants of a normal protein known as amyloid-β protein (Aβ); Aβ1-40 and Aβ1-42 are the predominant forms [1–3], and both form fibrils *in vitro* by a seeded polymerization mechanism [5]. The observation that nucleation of the Aβ1-42 fibril is significantly faster than that of the Aβ1-40 fibril led to the proposal that Aβ1-42 could be the pathogenic variant [5,6]. Consistent with this, it has since been demonstrated that all forms of rare, early-onset AD involve increased expression of Aβ1-42 [3]. Overproduction of Aβ1-42, however, does not appear to be a feature of most late-onset AD cases; in fact, the increased amyloid load in these patients is comprised primarily of Aβ1-40 [7].

In vitro studies have led to a simple cooperative two-state model of fibril formation in which only monomeric Aβ and fibrillar Aβ are significantly populated at any time during fibril formation [8]. In order to test this hypothesis, we utilized atomic force microscopy (AFM) to observe the early stages of amyloid fibril formation [9]. Because AFM provides a three-dimensional characterization of the fibril, it offers a distinct advantage over traditional electron microscopy [10]. For AFM analysis, the sample is adsorbed onto an atomically smooth surface (e.g., mica) and analyzed directly by sensing the adsorbed material with a microfabricated silicon tip attached to a sensitive cantilever [10]. The resulting relief map is subsequently converted into a visual image. The resolution of this method is limited by the size and shape of the tip; current microfabricated silicon tips (the tips used in this study) have an average radius of around 10–15 nm, although carbon nanotube tips that have smaller radii should enable significantly

higher resolution images to be obtained (S. Wong, J.D.H., P.T.L., and C.M.L., unpublished observations; [11]).

Although AFM has many advantages for studying fibril morphology, certain limitations must be taken into consideration when using AFM to study the pathway of fibril formation. First, as only adsorbed species are observed, one could fail to observe species that are prominent in solution. Because the relative population of adsorbed species may not reflect their relative abundance in solution, conclusions regarding the thermodynamics of the process cannot be drawn. The selective adsorption effect can be useful, however; for example, to trap a kinetically important species that is not abundant in solution and would be difficult to characterize using other methods. By observing the temporal evolution of selected Aβ-derived species, one can construct a testable mechanistic model of fibril formation. The potential exists, provided that several technical obstacles can be overcome, to utilize AFM to study the kinetics of assembly of a single, surface-attached species in aqueous buffer.

AFM images of early *in vitro* Aβ amyloid fibril formation have revealed the existence of a family of Aβ oligomers, of heterogeneous length, which differ from the much longer product fibrils with respect to their height and morphology [9,12]. These oligomers, collectively termed protofibrils, appear well before fibrils are observed, grow over a period of weeks in the absence of agitation (stirring significantly increases the rate of fibril formation [5,8,9,13]), and then disappear rapidly as fibrils grow [9,12]. The protofibril is approximately 3–4 nm in height and has a periodicity of ~20 nm, compared to the type 1 fibril (the first type of fibril to be observed) which has a height of 7–8 nm and a periodicity of ~40 nm. Two explanations for the transient appearance of the protofibril were put forward; the protofibril could be an off-pathway 'reservoir phase', in rapid equilibrium with monomeric Aβ, or an on-pathway assembly intermediate, from which fibrils are constructed [9,12]. In the latter case, the protofibril would also be expected to be the preferred substrate for fibril growth. The rapid transition from 100–200 nm protofibrils to fibrils of greater than 1 μm in length, which occurs after a relatively long period in which the protofibrils grow from 30–50 nm to 100–200 nm, suggests that the transition is cooperative and could be seeded by preformed fibrils [9]. Clarification of these issues could have important implications for the development of AD therapeutics and diagnostics.

Here we report the direct observation of the seeded polymerization of Aβ1-40 using AFM. These studies demonstrate that protofibrils do not seed fibril formation but are the preferred substrates for addition to pre-existing fibril seeds. In addition, the observation of branched fibril morphologies is reported, which suggests a mechanistic model for seeded fibril growth.

Results

Both Aβ1-40 and Aβ1-42 follow an analogous pathway to form the fibril, including the early appearance of protofibrils, followed by their elongation and eventual disappearance [9,12]. As fibrils form much faster in stirred incubations [5,9,13], the studies reported here were performed in the absence of agitation, to maximize our chances of observing early intermediates. In addition, the Aβ variant Aβ1-40, rather than Aβ1-42, was used because it is intrinsically less prone to form fibrils [5,9,12], making it easier to observe transient protofibrils. Although Aβ1-42 seems to be the pathogenic species in early-onset familial AD [3], increased deposition of Aβ1-40 is characteristic of late-onset AD patients bearing the apoE4 allele (apoE4 is a susceptibility factor for late-onset AD) [7].

Protofibril growth is dependent on time and concentration

Measurements of average protofibril length were made on aliquots removed from three Aβ1-40 samples (50, 100 and 200 μM). After 14 h, the average protofibril length at 50 μM Aβ1-40 was 55 nm (range 27–128 nm, 6% > 100 nm), at 100 μM, 69 nm (range 39–144 nm, 12% > 100 nm), and at 200 μM, 79 nm (range 27–291 nm, 23% > 100 nm, many > 150 nm). The 100 μM incubation was followed; after 63 h, the average protofibril length was 83 nm (range 30–242 nm, 30% > 100 nm), and after two weeks, the average length had reached 116 nm (range 20–595 nm, 50% > 100 nm, 10% > 200 nm, some protofibrils > 400 nm). The observed length distribution was not dependent on the duration of the interaction with the mica surface (data not shown). It has also been demonstrated that the amount of Aβ1-40 (and Aβ1-42) in protofibrillar form, like the average protofibril length, increases over time [12].

Fibril formation can be seeded by preformed fibrils but not by protofibrils

Addition of Aβ1-40 amyloid fibrils to a supersaturated solution of Aβ1-40 induces immediate polymerization, detected by a change in turbidity [5,13,14]. As observed by AFM, the conversion of protofibrils to amyloid fibrils was similarly accelerated by the addition of an aliquot from an Aβ1-40 incubation containing fibrils but no protofibrils. The total amount of Aβ1-40 in the seed aliquot was ~1% of the amount present in the supersaturated solution, Figure 1. Addition of an aliquot (containing the same amount of total Aβ1-40) from an incubation containing protofibrils, but no fibrils, had no effect (data not shown). In the seeded conversion, fibrils were clearly visible after 3 days; in the absence of seed, fibrils generally did not appear until at least 15 and usually >21 days had elapsed. Protofibrils were completely consumed in the seeded conversion by 14 days; in the absence of seed, protofibrils were visible after 30 days. Not all fibrillar preparations of Aβ1-40 were equally effective, suggesting that certain fibrillar morphologies are more effective seeds. This may explain why the observation of heterogeneous seeding of

Figure 1

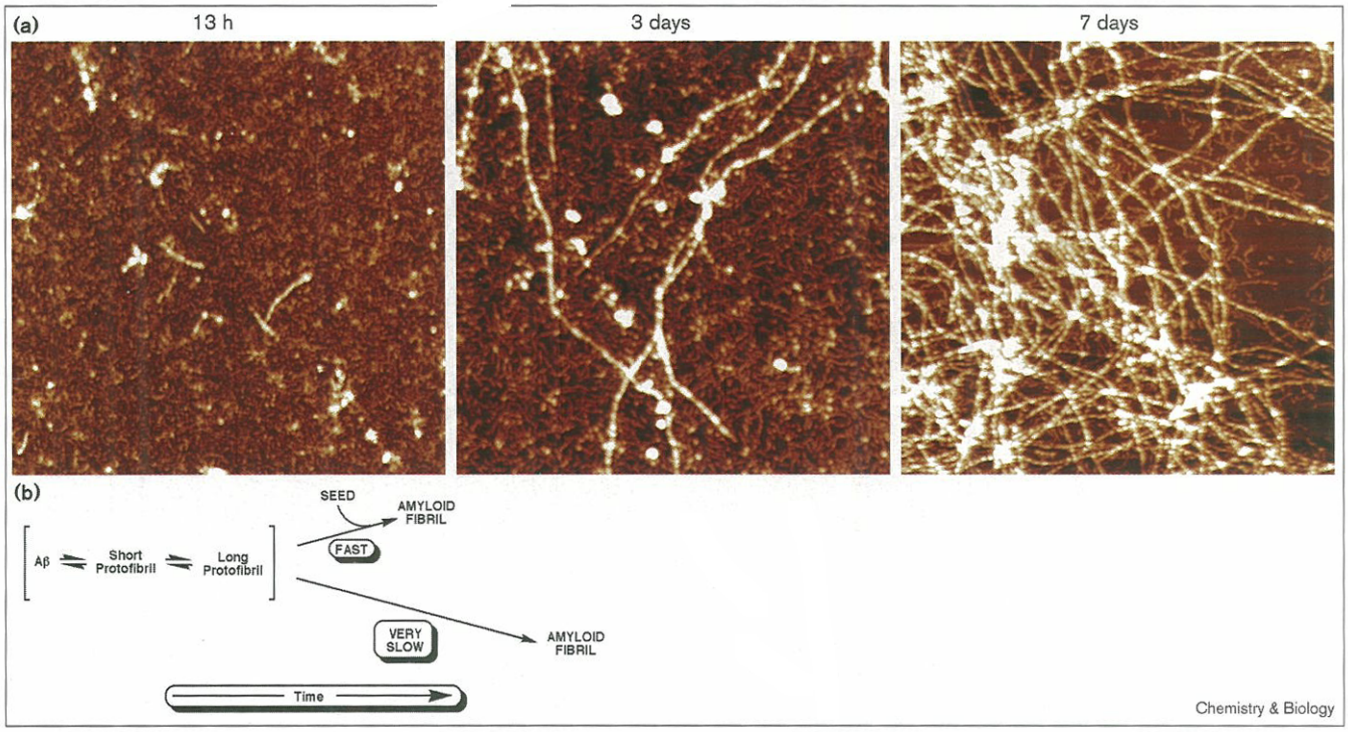

Fibrils seed the conversion of protofibrils to fibrils. **(a)** Three AFM images (2 μm square) taken at the indicated times following addition of ~1% preformed fibril seeds (based on initial Aβ1-40 concentration) to Aβ1-40 at 100 μM. An unseeded Aβ1-40 sample at the same concentration showed no evidence of of fibrils after 7 days (data not shown). **(b)** A mechanistic model, showing the key finding, that is preformed fibrils greatly accelerate the converison of protofibrils to fibrils.

100 μM Aβ1-40 by Aβ1-42 fibrils was inconsistent and depended on the source of Aβ1-42 fibrils [8].

The efficiency of seeded fibril growth depends on the amount and/or length of the protofibrils

The observation of seeded protofibril-to-fibril conversion (Figure 1) does not prove that protofibrils are on-pathway intermediates. In order to address whether this is the case, we investigated the relationship between protofibril formation/growth and the time course of the seeded conversion. As our methodology does not allow us to measure the amount of protofibrils, we instead focused on the average length of the observed protofibrils, which, like the amount of protofibrillar Aβ1-40 [12], increases over time (see above). If protofibrils are merely an off-pathway reservoir for Aβ, the efficiency of seeded conversion should be independent of the amount of protofibrils and/or their length. If the rate of Aβ dissociation from the protofibril is slow, however, seeded growth should be less effective as protofibril amount/length increases. AFM studies show that shortening of protofibrils on dilution occurs slowly (data not shown) and dialysis studies show that the protofibril-to-fibril transition is faster than protofibril dissolution (D. Walsh and D. Teplow, unpublished observations).

The opposite phenomenon was observed; that is, the seeded conversion of protofibrils to fibrils occurred much more rapidly from a preincubated sample containing longer protofibrils (Figure 2b; total [Aβ1-40] = 100 μM, preincubated for 13 days) compared to a sample containing short protofibrils but an equal Aβ1-40 total concentration (composed of monomeric Aβ plus protofibrillar Aβ plus all nonadsorbed species; Figure 2a, preincubated less than 5 minutes). One day after seeding of the long protofibrils sample, long (> 5 μm) fibrils were commonly observed and the amount of protofibrils had decreased significantly (Figure 2b); after 7 days, protofibrils were rare and fibril formation was essentially complete. In contrast, one day after seeding the preincubated sample, the solution remained unchanged except for the rare appearance of isolated fibrils (Figure 2a); protofibrils were still the predominant species after 7 days (in the absence of added seed, fibrils were not observed in the incubation containing short protofibrils after 7 days).

Fibrils have an inherent helical twist

Images of the type 1 fibril at high magnification (Figure 3a) clearly show a left-handed helical orientation to the periodic height increases (period = ~43 nm) along the length of the fibril. It is possible that simple beaded

Figure 2

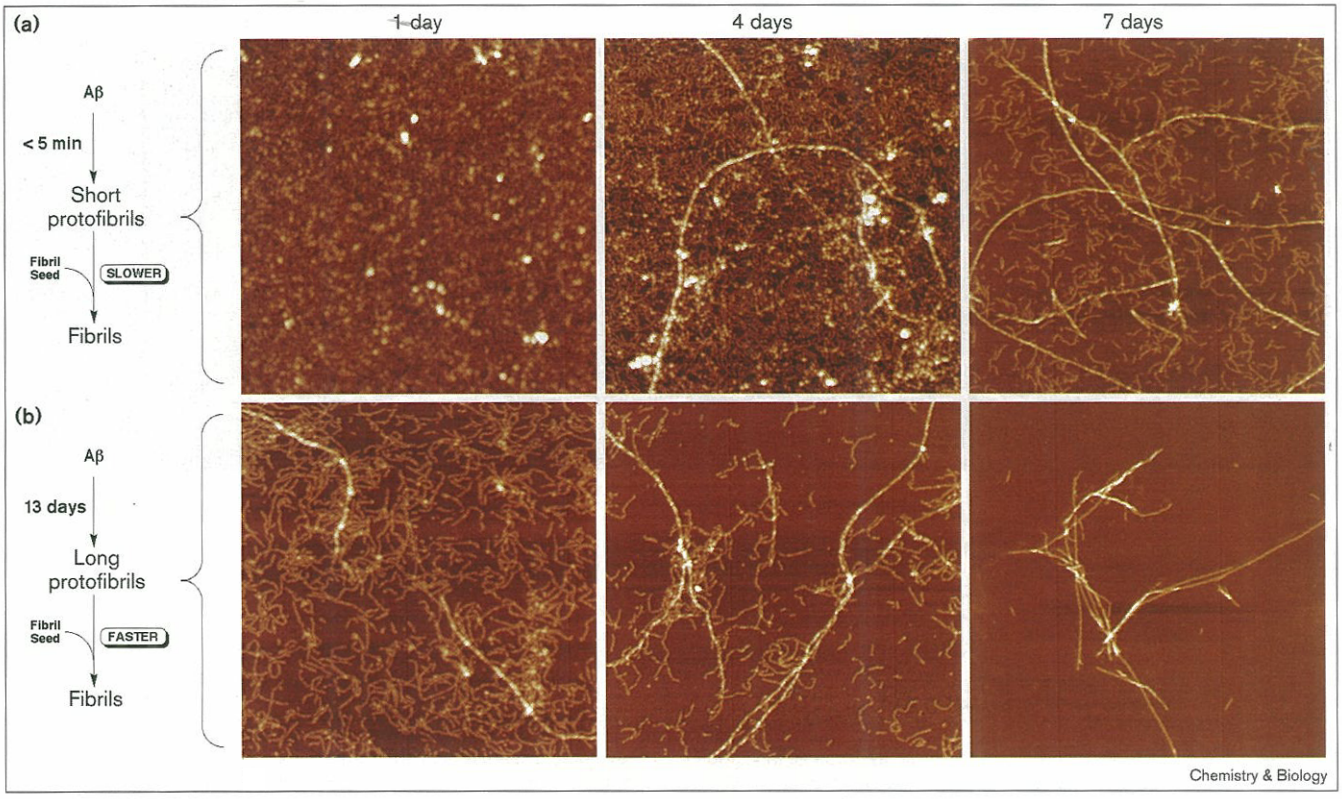

The efficiency of seeding depends on protofibril length. Aβ1-40 was preincubated at 100 μM for 5 min **(a)** or 13 days **(b)**, then identical amounts (~1% of the initial Aβ1-40 concentration) of preformed fibrils from the same source were added to seed the conversion to fibrils. An incubation containing monomeric Aβ and short protofibrils was slowly converted to fibrils (a), whereas an incubation containing long protofibrils was rapidly converted (b). All images are 2 μm square.

objects could have a helical appearance if the tip used to scan them was irregularly shaped, but two separate observations rule out this possibility. First, the observed helicity is the same regardless of the orientation of the fibrils in the image. Furthermore, type 1 fibrils formed by all-D Aβ1-40 showed identical periodicity of the height increases and were also clearly helical (Figure 3b), but the twist direction was always observed to be right-handed.

The seeding behavior of the enantiomeric fibrils was also examined. Aliquots of protofibrils formed by each enantiomer were separately seeded by adding fibril suspensions (5% of the initial Aβ concentration) formed by either the same or the opposite enantiomer. Acceleration of fibril formation was only observed when the fibrillar seed material was formed by the same enantiomer of Aβ1-40 as the protofibrils. This is consistent with previous observations of amyloid seeding specificity (reviewed in [2]).

Branched type 1 fibrils were observed

Branched type 1 fibrils were also observed (Figures 2, 4). At some branch points, both of the 'daughter' fibrils resembled type 1 fibrils (Figure 4a). At others, one of the daughter fibrils had a different morphology (Figure 4c; see discussion below). Although amyloid fibrils are typically described as unbranched, light scattering data have been interpreted to reflect a low degree of Aβ1-40 fibril branching under certain conditions [15].

Partially wound/unwound type 1 fibrils and constituent rigid filaments were observed

As the protofibril disappeared over time, type 1 fibrils became the predominantly observed species. The ends of type 1 fibrils were often characterized by staggered filament termination (Figure 4a; also observed in high resolution AFM studies using multiwalled carbon nanotube probes; S. Wong, J.D.H., P.T.L., and C.M.L., unpublished observations). Isolated rigid filaments (Figure 4b) and junctions between type 1 fibrils and two diverging filaments (Figures 4, 5) were also observed but only at late incubation times when protofibrils were no longer present. These filaments were ~40% the height of type 1 fibrils (3–4 nm), similar to Aβ1-40 protofibrils [9]. The filaments, however, were morphologically distinct from protofibrils,

Figure 3

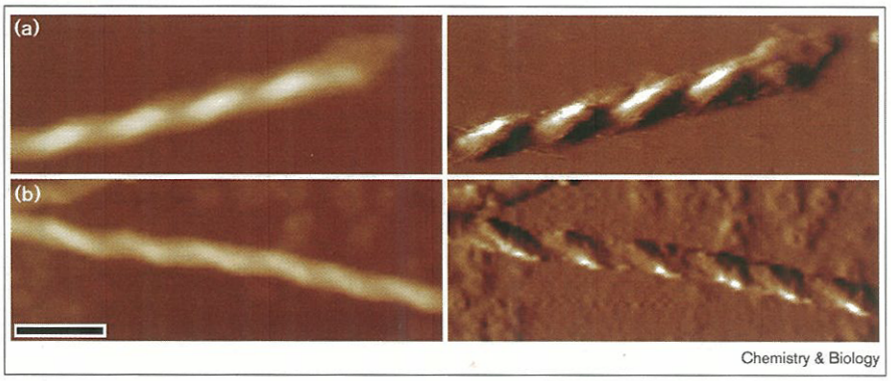

Helicity of type 1 fibrils. **(a)** Details of a type 1 fibril formed by all-L Aβ1-40. The helical nature of the periodic height increases (period ~43 nm) along the length of the fibril in the height data image on the left (brighter areas indicate taller features) and the fibril is clearly resolved as left-handed in the image on the right. This image was generated by plotting simultaneously acquired cantilever oscillation amplitude data which emphasize that rapid changes in height – bright areas correspond to decreases and dark areas to increases in cantilever oscillation amplitude during the scan. **(b)** Details of a type 1 fibril formed by all-D Aβ1-40. The periodicity of these fibrils is identical to those formed by the all-L peptide and also clearly has a helical orientation which is emphasized in the amplitude image on the right. For all-D Aβ1-40, however, the observed helicity is right-handed. Although the fibrils appear to have different widths, the heights of adsorbed type 1 fibrils formed by each peptide are indistinguishable, and width differences of this magnitude are consistent with variations in broadening artifacts caused by differences in tip shape. Scale bar = 50 nm.

as they had a 40 nm periodic substructure (protofibrils have a 20 nm periodicity), appeared to be rigid (protofibrils appeared to be flexible), and were often longer than 1 μm (protofibrils were usually < 200 nm [9]). Type 1 fibril/filament junctions may represent trapped, partially wound or unwound type 1 fibrils that exist at least transiently in solution. Isolated rigid filaments may result from complete unwinding of type 1 fibrils.

Discussion

The AFM studies reported here allowed the observation of a subpopulation of Aβ-derived species (the adsorbable species) at time points during fibril assembly. As all species may not be equally well adsorbed, it is not possible to determine the relative stability of these species on the basis of their abundance, nor is it possible to rule out the existence of other species that might be very poorly adsorbed. In order to test the possibility that selective adsorption may bias our observations, we have performed initial experiments using hydrophobic, highly ordered pyrolytic graphite surfaces rather than hydrophilic mica surfaces. The same Aβ1-40-derived species and no additional species were detected (data not shown). Although it is possible that adsorption traps species that are normally

Figure 4

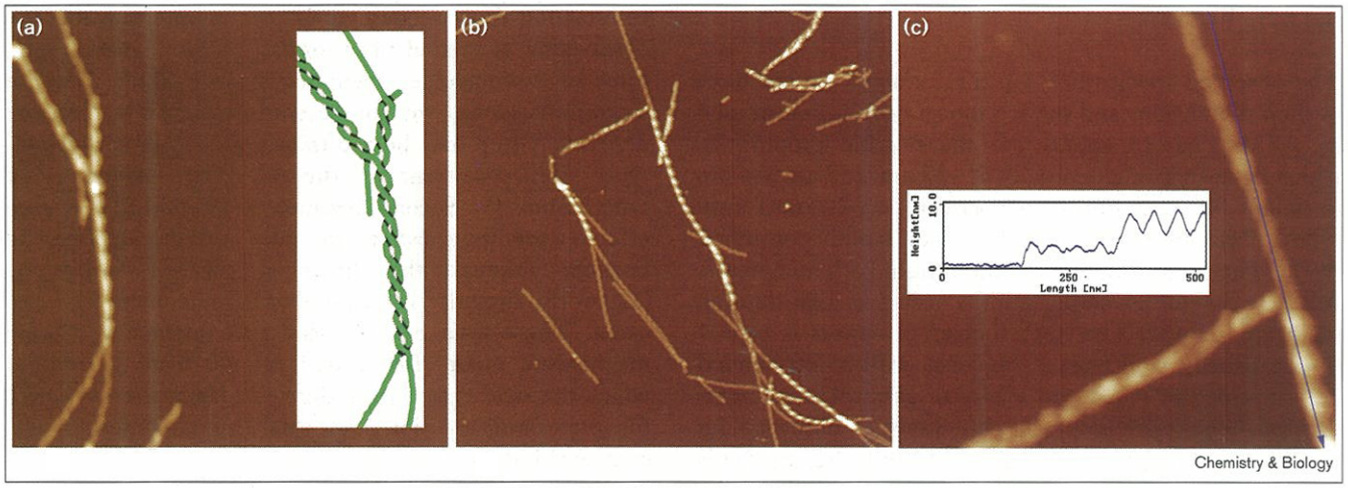

Winding/unwinding and branching of Aβ1-40 fibrils. **(a)** A fibril that is partially wound at one end and branched at the other (1 μm square). The inset shows a schematic interpretation of the morphology. **(b)** Fibril unwinding and branching (2 μm square). **(c)** An enlargement of a central region of (b), showing branching in more detail (500 nm square). The inset shows a cross-section along the indicated plane (blue arrow) that clearly shows the transition from 3–5 nm single filament to 7–9 nm type 1 fibril.

Figure 5

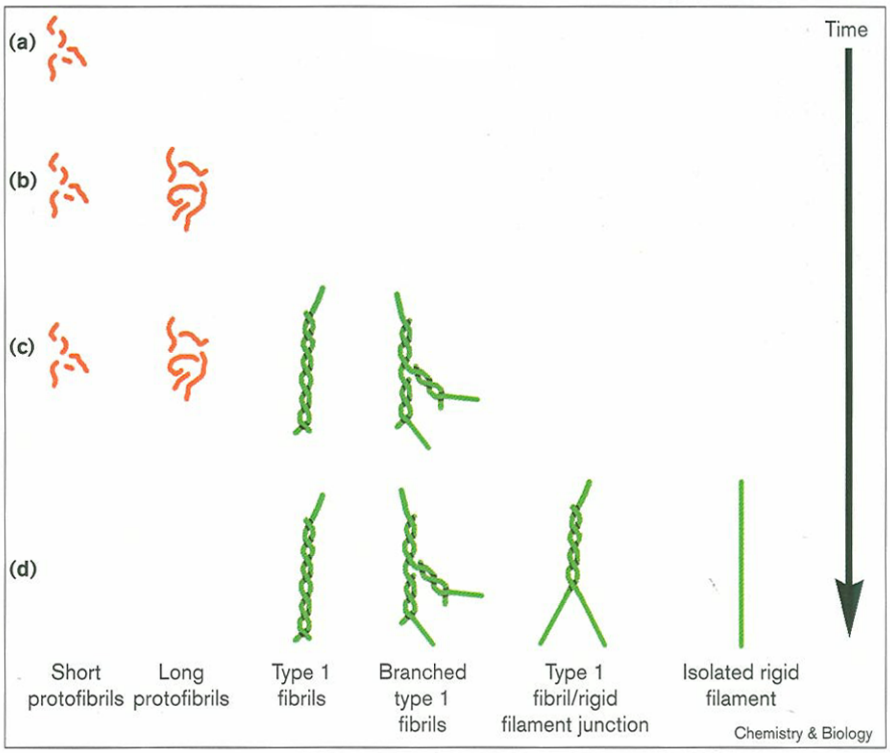

The temporal evolution of Aβ1-40-derived species. **(a)** At the earliest time points, the only observed Aβ1-40 aggregates are short protofibrils [9]. **(b)** Subsequently, longer protofibrils become increasingly common. **(c)** After 3–4 weeks, or 1–7 days following the addition of preformed fibrils, both protofibrils and long type 1 fibrils are seen. Branching of fibrils is frequently observed at this stage (see days 4 and 7 in Figure 2). Changing color from red for protofibrils to green for fibrils reflects a putative conformational change suggested by the increased rigidity and different periodicity of filaments compared to protofibrils. **(d)** In the late stages, protofibrils are no longer observed. In addition to type 1 fibrils and branched type 1 fibrils, isolated rigid filaments and junctions are observed.

sparsely populated in solution (e.g., unwound type 1 fibrils), the observation of these potentially kinetically important species may provide clues as to the mechanism of fibril assembly. Using alternative methods, Teplow and co-workers [12] have recently determined that a significant proportion of total soluble Aβ is rapidly converted to a protofibrillar species, which subsequently disappears as dense, highly insoluble fibrils form. The temporal evolution of the Aβ1-40-derived species imaged in this work is shown in Figure 5.

The observed species fall into three classes, on the basis of their dimensions and surface topography as determined by AFM. First to appear are the flexible protofibrils, which have an axial periodicity of ~20 nm, and are 3–4 nm in height [9]. Protofibrils grow slowly (to ~200 nm) until type 1 fibrils are observed, and are then rapidly consumed [9,12]. The protofibrils are in equilibrium with monomeric Aβ; slow dissolution of protofibrils occurs at high dilution (data not shown). The next species to appear is type 1 fibrils; usually well over 1 μm long, with a left-handed helical structure (axial periodicity of about 43 nm; right-handed helicity of identical periodicity is observed for type 1 fibrils comprising all-D Aβ1-40), and a height that is approximately 2.5 times that of the protofibril. After the protofibrillar population has been consumed, filaments appear that are rigid and long like type 1 fibrils, have axial periodicity resembling the type 1 fibril, but have a height that is indistinguishable from the protofibril. The helicity and dimensions of the type 1 fibril and the dimensions of the rigid and long filaments are consistent with a two-filament wound morphology for the type 1 fibril. There is a well established precedent for the two-filament wound morphology (see below). The morphological differences between the rigid filaments and the flexible protofibrils may reflect a critical conformational change (red to green in Figure 6).

Information about seeded growth can be inferred from the observation of seeded fibril formation. First, as only mixtures of morphologies including type 1 fibrils, but not protofibrils alone, are competent seeds, the nucleation-dependent step may be the transition from protofibril-to-type 1 fibril, consistent with the sudden appearance of long type 1 fibrils [9]. Second, because the protofibril is a more effective seeding substrate, its addition to the seed may be favored, although the direct addition of monomeric [12,16–18], dimeric [12], or higher Aβ oligomers may also occur. These data can be used to construct a testable mechanistic model for seeded Aβ1-40 fibril growth, in which the rigid type 1 fibril-derived filament acts as a site for protofibril addition and catalyzes a conformational change (Figure 6; [19]).

Although these studies were conducted under conditions that differ from those under which fibril formation is initiated *in vivo* [1,4,8,14], three facts support the relevance of the *in vitro* process. First, protofibril formation has been

Figure 6

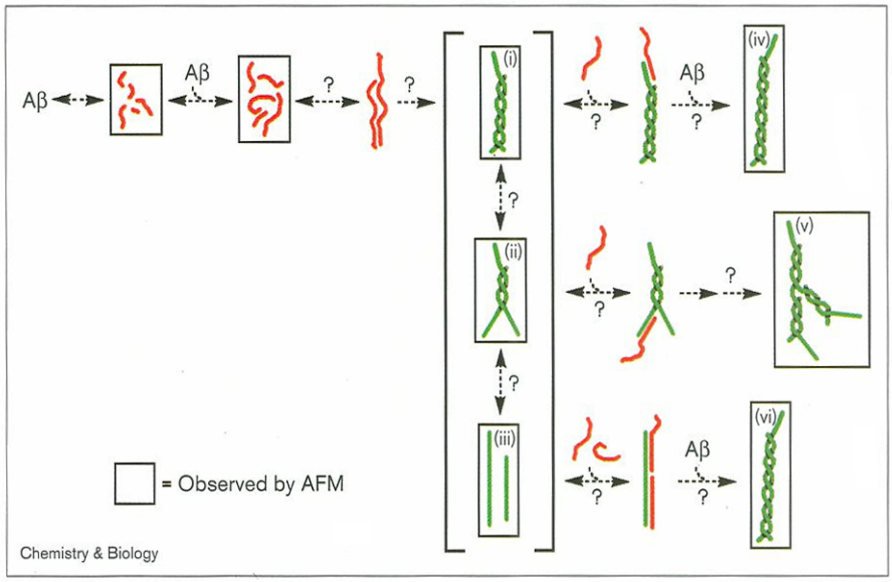

A working hypothesis to explain seeded amyloid fibril growth. Oligomeric Aβ species that have been directly observed by AFM (see Figure 5) are shown in boxes. Inferred species (unboxed) and hypothetical pathways to explain the interconversion of species (dashed arrows with question marks) are included. In the earliest stages of fibril formation, monomeric (or dimeric [12]) Aβ rapidly oligomerizes to form short protofibrils. The average length of the observed protofibrils (and the total amount [12]) increases with time. Nucleus formation may involve annealing, winding, and an irreversible conformational change (red to green) to produce a type 1 fibril. The conformational change provides an explanation for the apparent cooperativity of fibril formation and could lead to a preorganized single filament seed template that is an optimal binding site for addition of a subsequent protofibril. The addition of seed containing a mixture of fibrillar species (shown in square brackets) bypasses nucleation. An exposed rigid filament could seed growth by catalyzing the conformational change in an added protofibril, analogous to flagellar assembly [19]. Fibril morphologies with exposed rigid filaments could arise if protofibrils with different lengths or offset alignments associate and wind to produce a fibril end with staggered termination of filaments (i), or if fibril ends can transiently or completely unwind (ii,iii) to expose single filament templates. Addition of a protofibril to an exposed filament could lead to unbranched elongation of a type 1 fibril (iv,vi), or to branched morphology (v). Fibril elongation may also occur by addition of Aβ monomer/small Aβ oligomer onto filament ends [12,16–18]. Detailed kinetic studies, utilizing multiple methods to characterize and quantify all intermediates [8,12–14], are required to test this model.

observed under a variety of conditions; second, AD brain-derived amyloid fibrils have a two-filament wound morphology; and third, amyloid fibrils comprising other proteins have a similar wound morphology. Since the concentration of Aβ, averaged throughout the brain, is well below the critical concentration (the concentration of Aβ below which fibrils do not form) [8], the site of *in vivo* amyloid growth is likely to be a cellular compartment, where Aβ is locally concentrated. We have observed protofibril formation *in vitro* at Aβ1-40 concentrations that approach the critical concentration of ~30 μM [9] and over a range of ionic strengths, pHs, and buffer compositions (J.D.H., unpublished observations).

The morphological similarities of brain-derived fibrils to those formed *in vitro* also support the relevance of the *in vitro* studies reported here. Amyloid fibrils, observed in AD brain tissue sections by electron microscopy, seem to be composed of two wound 4–7 nm diameter filaments [20,21]. Miyakawa *et al.* [22] propose a hollow-centered bundle of helically wound subunits; however, their data are also consistent with the winding of two semicylindrical filaments. Amyloid preparations extracted from AD brain also have a wound morphology; Roher *et al.* [23,24] observed ~5 nm wide filaments, in addition to typical 10 nm wide fibrils, suggesting winding/unwinding. Merz *et al.* [20] noted a 40 nm periodicity in the 10 nm wide fibrils, reminiscent of the Aβ1-40 type 1 fibrils formed *in vitro* by our group [9]. The 40 nm periodicity and branching also characterized Aβ1-40 fibrils produced *in vitro* by another laboratory [25].

Fibrils that characterize other amyloid diseases comprising other peptides and proteins share some of these features. Amyloid fibrils of the prion protein, isolated from the brains of human and rodent scrapie cases, are characterized by a two-filament wound morphology [20]. Transthyretin amyloid fibrils seem to be composed of bundles of four 'protofilaments', each of which has been proposed to consist of two wound filaments (the twist periodicity is ~11.5 nm; [26]). Fibrils comprising islet amyloid polypeptide (the major constituent of pancreatic amyloid that characterizes type II diabetes) and the peptide calcitonin (~8 nm diameter) have also been proposed to be derived from annealing and winding of protofibrils [27,28]. Finally, cytokeratin fibrils (reconstituted from purified cytokeratin isolated from fibrillar deposits in diseased livers) have a similar twisted filament morphology (~40 nm periodicity) and have also been observed to partially wind/unwind [29].

In order to demonstrate unequivocally the importance of the transient species reported here, the same species must be identified in, or extracted from, AD brain tissue. Protofibrils are most likely to be found in the brains of individuals predisposed to develop AD, such as young Down's syndrome [30] and head trauma patients [31]. In

both of these groups, significant deposition of Aβ, in a nonfibrillar form called diffuse amyloid, precedes symptoms [30,31]. Diffuse amyloid has been proposed to be a precursor of fibrillar amyloid [32], and contains protofibrils [9]. Significantly, the *in vitro* neurotoxicity of commercial Aβ1-40 seems to be inversely correlated with the prevalence of nonfibrillar species that we believe are protofibrils [25]. This finding suggests that inhibition of the protofibril-to-fibril transition may prevent *in vivo* neurodegeneration [4].

Significance

Accumulating evidence indicates that the formation of amyloid plaques in the brain is a central event in Alzheimer's disease (AD) pathogenesis. The plaques are primarily composed of the fibrillar form of the amyloid-β protein (Aβ). In this study, atomic force microscopic images of seeded Aβ fibril growth *in vitro* show that fibril growth can be seeded by the addition of preformed fibrils, but not by preformed protofibrils, and that protofibrils are incorporated into growing fibrils. New morphological features, including fibril branching and fibril winding/unwinding, have been observed, and the helicity of fibrils has been demonstrated. This information provides the basis for a testable model for seeded fibril growth *in vitro*. In this model, the nucleation-dependent step occurs during the transition of protofibrils-to-fibrils and exposed single filaments act as a template for annealing, winding and rigidification of protofibrils during fibril growth.

The direct role of the protofibril in type 1 fibril formation *in vitro* strongly suggests that the protofibril also plays an important role in the formation of the morphologically indistinguishable amyloid fibrils in the brains of individuals with AD. Protofibrils would be expected to form early in AD, possibly preceding the death of neurons and the appearance of symptoms. Agents that inhibit the protofibril-to-fibril transition of Aβ *in vitro* may lead the way to developing therapeutic agents to combat AD.

Materials and methods

Protein substrate

Synthetic Aβ1-40 was purchased from Quality Controlled Biochemicals Inc. (Hopkinton, MA). Synthetic Aβ1-40 made using all-D amino acids was provided by Michael Vitek (Duke University).

Preparation of seed-free Aβ1-40 stock solutions

Stock solutions of Aβ1-40 in dimethyl sulfoxide (DMSO) were prepared at a concentration of approximately 12 mg/ml. The peptide solution was then sonicated for 5–10 min and filtered through a 0.2 μm nylon microspin filter (Whatman Inc., Clifton, NJ) to remove any undissolved seed. Final peptide concentrations of the DMSO stock solutions, as determined by quantitative amino analysis, were typically 2–2.5 mM.

In vitro *aggregation of Aβ1-40*

Aβ aggregation was initiated by adding an aliquot of a concentrated DMSO stock of Aβ1-40 to aqueous buffer (10 mM phosphate, 137 mM NaCl, 27 mM KCl, pH 7.4) followed by immediate vortexing to mix thoroughly. The concentration of DMSO in the aggregation buffer was kept constant ($\leq$ 5% by volume) by adding DMSO to the sample buffer of the less concentrated Aβ1-40 solutions. After initial mixing the solutions were incubated at room temperature without further agitation except for gentle tapping to ensure homogeneous aliquots for AFM.

Seeding experiments

100 μM solutions of Aβ1-40, containing long protofibrils (after > 1 week preincubation) were divided in two. One portion was left unaltered and the other portion was seeded by adding preformed seed fibrils and filaments ($\leq$ 1% of a molar equivalent based on initial total [Aβ1-40]), but no protofibrils (morphology confirmed by AFM just prior to use). At the same time, a 100 μM Aβ1-40 solution that was not preincubated was also seeded with the same amount of the identical seed stock. The seed stock was diluted into buffer containing no Aβ1-40 and imaged to determine the contribution of seed fibrils to the observed images; no fibrils were detected, indicating that the observed fibrils in the seeded growth incubations are attributable to new growth, rather than the seed aliquot.

Atomic force microscopy

The incubating samples were mixed by gentle tapping to evenly suspend any aggregates, and 3–5 μl aliquots were placed on freshly cleaved mica (Ted Pella, Redding, CA). After 30 s, the mica was gently rinsed twice with 50 μl of 0.2 μm-filtered water to remove salt and loosely bound peptide. Excess water was removed with a gentle stream of filtered compressed tetrafluoroethane, and the samples were imaged immediately. All images were obtained under ambient conditions with a Nanoscope IIIa Multimode scanning probe workstation (Digital Instruments, Santa Barbara, CA) operating in TappingMode™ using etched silicon NanoProbes™ (Probe Model TESP, Digital Instruments). Scanning parameters varied with individual tips and samples, but typical ranges were as follows: initial root mean square (RMS) amplitude, 1.2 V; setpoint, 0.9–1.1 V; tapping frequency, 250–350 kHz; scan rate, 0.8–1.75 Hz.

Measurement of Aβ oligomer dimensions

Protofibril length average. Aliquots were diluted to 20 μM Aβ1-40 immediately prior to sample preparation to allow individual protofibrils to be discerned and measured. Consecutive scans were monitored until distortion due to creep or shifts in the slow scan direction were negligible. An area containing 50–70 protofibrils was chosen, and all protofibrils within this region were measured by summing the lengths of short line segments (in top view mode in the Nanoscope software) drawn to approximate the curvature of the protofibrils (globular aggregates measuring $\leq$ 20 nm and showing no evidence of elongation were counted in each region, but were not included in protofibril length averages).

Comparison of morphology heights. Because variations in sample hydration, scanner calibration, and applied forces during imaging can alter the observed dimensions of protein samples, quantitative height comparisons are based on data obtained from single scans of regions where the morphologies to be compared both appear. To allow height comparison between protofibril and filament (which are not clearly observed together in single scans), the average fibril (type 1) height (present with protofibrils and filaments) was used as an internal height calibration standard. Cross sections of features were made perpendicular to the long axis of the feature at periodic height maxima to obtain feature height averages (at least 30 measurements of separate cross sections for each average).

Periodicity measurements. Averages of 30 separate peak-to-peak distances were made for each morphology with observed regular periodicities.

Acknowledgements

This work was supported by the National Institutes of Health (AG08470), an NIH Biotechnology training grant (J.D.H.), and the Foundation for Neurologic Diseases (Newburyport, MA). We thank David Teplow and Dominic Walsh of the Center for Neurologic Diseases for sharing unpublished results with us, and Michael Vitek of Duke University for providing all-D Aβ1-40.

References

1. Yankner, B.A. (1996). Mechanisms of neuronal degeneration in Alzheimer's disease. *Neuron* **16**, 921-932.
2. Lansbury, P.T., Jr. (1996). A reductionist view of Alzheimer's disease. *Accounts Chem. Res.* **29**, 317-321.
3. Selkoe, D.J. (1997). Alzheimer's disease: genotypes, phenotype, and treatments. *Science* **275**, 630-631.
4. Lansbury, P.T., Jr. (1997). Inhibition of amyloid formation: a strategy to delay the onset of Alzheimer's disease. *Curr. Opin. Chem. Biol.* **1**, 260-267.
5. Jarrett, J.T., Berger, E.P., & Lansbury, P.T., Jr. (1993). The carboxyl terminus of β amyloid protein is critical for the seeding of amyloid formation: implications for the pathogenesis of Alzheimer's disease. *Biochemistry* **32**, 4693-4697.
6. Cai, X.D., Golde, T.E., & Younkin, S.G. (1993). Release of excess amyloid β protein from a mutant amyloid β protein precursor. *Science* **259**, 514-516.
7. Gearing, M., Mori, H., & Mira, S. (1996). Aβ-peptide length and apolipoprotein E genotype in Alzhiemer's disease. *Ann. Neurol.* **39**, 395-399.
8. Harper, J.D., & Lansbury, P.T., Jr. (1997). Models of amyloid seeding in Alzheimer's disease and scrapie: Mechanistic truths and physiological consequences of the time-dependent solubility of amyloid proteins. *Annu. Rev. Biochem.* **66**, 385-407.
9. Harper, J.D., Wong, S.S., Lieber, C.M., & Lansbury, P.T., Jr. (1997). Observation of metastable Aβ amyloid protofibrils by atomic force microscopy. *Chem. Biol.* **4**, 119-125.
10. Bustamante, C., & Keller, D. (1995). Scanning force microscopy in biology. *Physics Today* 32-38.
11. Dai, H., Hafner, J.H., Rinzler, A.G., Colbert, D.T., & Smalley, R.E. (1996). Nanotubes as nanoprobes in scanning probe microscopy. *Nature* **384**, 147-150.
12. Walsh, D.M., Lomakin, A., Benedek, G.B., Comdron, M.M., & Teplow, D.B. (1997). Amyloid β-protein fibrillogenesis: detection of a protofibrillar intermediate. *J. Biol. Chem.* **272**, 22364-22372.
13. Wood, S.J., Chan, W., & Wetzel, R. (1996). An ApoE-Aβ inhibition complex in Aβ fibril extension. *Chem. Biol.* **3**, 949-956.
14. Wood, S.J., Maleeff, B., Hart, T., & Wetzel, R. (1995). Physical, morphological and functional differences between pH 5.8 and 7.4 aggregates of the Alzheimer's amyloid peptide A-beta *J. Mol. Biol.* **256**, 870-877.
15. Shen, C.L., & Murphy, R.M. (1995). Solvent effects on self-assembly of β-amyloid peptide. *Biophys. J.* **69**, 640-651.
16. Maggio, J.E., et al., & Mantyh, P.W. (1992). Reversible *in vitro* growth of Alzheimer's disease β-amyloid plaques by deposition of labeled amyloid peptide. *Proc. Natl Acad. Sci. USA* **89**, 5462-5466.
17. Naiki, H., Higuchi, K., Nakakuki, K., & Takeda, T. (1991). Kinetic analysis of amyloid fibril polymerization *in vitro*. *Lab. Invest.* **65**, 104-110.
18. Naiki, H., & Nakakuki, K. (1996). First-order kinetic model of Alzheimer's β-amyloid fibril extension *in vitro*. *Lab. Invest.* **74**, 374-83.
19. Asakura, L. (1970). Polymerization of flagellin and polymorphism of flagella. *Adv. Biophys.* **1**, 99-155.
20. Merz, P.A., Wisniewski, H.M., Somerville, R.A., Bobin, S.A., Masters, C.L., & Iqbal, K. (1983). Ultrastructural morphology of amyloid fibrils from neuritic and amyloid plaques. *Acta Neuropathol.* **60**, 113-124.
21. Narang, H.K. (1980). High-resolution electron microscopic analysis of the amyloid fibril in Alzheimer's disease. *J. Neuropath. Exp. Neurol.* **39**, 621-631.
22. Miyakawa, T., Watanabe, K., & Katsuragi, S. (1986). Ultrastructure of amyloid fibrils in Alzheimer's disease and Down's syndrome. *Virchows Arch. B Cell Pathol. Incl. Mol. Pathol.* **52**, 99-106.
23. Roher, A., Wolfe, D., Palutke, M., & KuKuruga, D. (1986). Purification, ultrastructure, and chemical analysis of Alzheimer's disease amyloid plaque core protein. *Proc. Natl Acad. Sci. USA* **83**, 2662-2666.
24. Roher, A.E., Palmer, K.C., Yurewicz, E.C., Ball, M.J., & Greenberg, B.D. (1993). Morphological and biochemical analysis of amyloid plaque core proteins purified from AD brain tissue. *J. Neurochem.* **61**, 1916-1926.
25. Howlett, D.R., et al., & Roberts, G.W. (1995). Aggregation state and neurotoxic properties of Alzheimer beta-amyloid peptide. *Neurodegeneration* **4**, 23-32.
26. Blake, C., & Serpell, L. (1996). Synchrotron X-ray studies suggest that the core of the transthyretin amyloid fibril is a continuous β-sheet helix. *Structure* **4**, 989-998.
27. Goldsbury, C.S., et al., & Kistler, J. (1997). Polymorphic fibrillar assembly of human amylin. *J. Struct. Biol.* **119**, 17-27.
28. Bauer, H.H., et al., & Merkle, H.P. (1995). Architecture and polymorphism of fibrillar supramolecular assemblies produced by *in vitro* aggregation of human calcitonin. *J. Struct. Biol.* **115**, 1-15.
29. Pollanen, M.S., Markiewicz, P., Weyer, L., Goh, M.C., & Bergeron, C. (1994). Mallory body filaments become insoluble after normal assembly into intermediate filaments. *Am. J. Pathol.* **145**, 1140-1147.
30. Lemere, C.A., Blusztajn, H., Yamaguchi, H., Wisniewski, T., Saido, T.C., & Selkoe, D.J. (1996). Sequence of deposition of heterogeneous amyloid β-peptides and APO E in down syndrome: Implications for initial events in amyloid plaque formation. *Neurobiol. Dis.* **3**, 16-32.
31. Nicoll, J.A.R., Roberts, G.W., & Graham, D.I. (1995). Apolipoprotein E epsilon 4 allele is associated with deposition of amyloid β-protein following head injury. *Nat. Med.* **1**, 135-137.
32. Selkoe, D.J. (1994). Normal and abnormal biology of the beta-amyloid precursor protein. *Annu. Rev. Neurosci.* **17**, 489-517.